Lab on a Chip

PAPER

View Article Online
View Journal | View Issue

Cite this: *Lab Chip*, 2025, **25**, 4800

Groove-aided sacrificial molding for fabrication of an *in vitro* vascular model with branches using ECM-derived materials

Jumpei Muramatsu,[a] Michinao Hashimoto,[b] Shigenori Miura[c] and Hiroaki Onoe[*d]

Received 1st March 2025,
Accepted 27th July 2025

DOI: 10.1039/d5lc00214a

rsc.li/loc

This paper describes a fabrication method of an *in vitro* branched vascular model using extracellular matrix (ECM)-derived materials (transglutaminase crosslinked gelatin, TG-gelatin). Mechanical stresses, such as disturbed blood flow derived from vascular branches, are a significant cause of cardiovascular disease. To study cardiovascular diseases, a perfusion and stretching culture platform with an ECM-based *in vitro* vascular model with branches has been essential. Among the proposed microchannel fabrication methods, sacrificial molding with a template made of soluble material is attractive for fabricating branched microchannels. However, the soluble template remained an issue of undesired deformation due to the swelling caused by the moisture in the hydrogel. Here, we propose groove-aided sacrificial molding (GAS molding) to suppress the deformation of the soluble template in the TG-gelatin. By preparing a channel-shaped groove on the TG-gelatin, the shape retention of the soluble template is assisted. We experimentally evaluated the deformation of the microchannels fabricated by the proposed GAS molding. The vascular endothelial cells were seeded into microchannels fabricated by GAS molding for perfusion and stretching culture. The effects of mechanical stress were visualized by immunofluorescence staining of PECAM1 and integrin α9 in the endothelial cells. Overall, our method would suggest a platform to spatially elucidate the cellular responses to irregular mechanical stresses, such as triggers of cardiovascular disease.

Introduction

Blood vessels are essential organs for humans to supply oxygen and nutrients to the tissues in the body and to collect waste products from the tissues. In the blood vessels, severe cardiovascular diseases such as myocardial infarction, ischaemic heart disease, and stroke are significant causes of death in humans.[1,2] One of the major causes of these cardiovascular diseases is mechanical stress on the inner walls of blood vessels, especially disturbed blood flow at branches or bends.[3,4] However, the details of the relationship between disturbed mechanical stress and the development of cardiovascular disease are still unknown. To elucidate the relationship between them, *in vitro* vascular models with cultured endothelial cells under mechanical stresses have been developed.[5–7] For an *in vitro* vascular model mimicking the *in vivo* vascular environment, it is essential to have an extracellular matrix (ECM) scaffold to imitate the stiffness of the scaffold *in vivo* and to have branched channels to generate heterogeneous mechanical stress.[8–11] Nevertheless, the existing *in vitro* ECM-based vascular models were primarily limited to straight tubes due to direct molding, such as extracting wires.[5–7] Hence, fabrication methods for branched *in vitro* ECM-based vascular models have been the focus recently.

For fabrication of ECM-based *in vitro* vascular models, soft lithography,[12,13] mold extracting,[14,15] and three-dimensional (3D) bioprinting[16,17] are widely used. Notably, sacrificial molding, in which a mold made of soluble materials is dissolved to form microchannels in an ECM-based scaffold, is practical for fabricating microchannels of the designed shape.[18–20] An overview of the general sacrificial molding process is as follows: firstly, a designed channel-shaped sacrificial template, commonly made of water-soluble[21,22] or decomposable[23,24] polymers, is prepared. Secondly, the sacrificial template is embedded in the ECM scaffold and dissolved to form the designed microchannels. The materials for sacrificial templates have two requirements: (i) keeping

[a] *School of Integrated Design Engineering, Graduate School of Science and Technology, Keio University, 25-202, 3-14-1 Hiyoshi, Kohoku-ku, Yokohama, Kanagawa 223-8522, Japan*
[b] *Pillar of Engineering Product Development, Singapore University of Technology and Design, 8 Somapah Road, Singapore 487372, Singapore. E-mail: hashimoto@sutd.edu.sg*
[c] *Department of Molecular Biology and Biochemistry, Graduate School of Biomedical and Health Sciences, Hiroshima University, 1-2-3 Kasumi, Minami-ku, Hiroshima City, Hiroshima 734-8553, Japan. E-mail: miuras@hiroshima-u.ac.jp*
[d] *Department of Mechanical Engineering, Faculty of Science and Technology, Keio University, 25-202, 3-14-1 Hiyoshi, Kohoku-ku, Yokohama, Kanagawa 223-8522, Japan. E-mail: onoe@mech.keio.ac.jp*

the template shape in the scaffold and (ii) being dissolved by enzymes or reagents under tissue-friendly conditions. Alginate hydrogels[25,26] and sugar-based materials[27,28] have been fascinating soluble materials for sacrificial templates, though the patterning capability of these materials needs to be improved to the scale of precise blood vessels. On the other hand, water-soluble support materials for fused deposition modelling (FDM) 3D printers have attracted attention (especially polyvinyl alcohol (PVA)[29–32]). PVA is widely used as a water-soluble sacrificial material for FDM 3D printing, and PVA-based sacrificial templates can be deposited in a designed 3D shape on a substrate in air and easily dissolved in water. Hence, sacrificial templates with support materials have the potential to expand the flexibility of designing branched vascular microchannels.[30–32] However, the support materials for FDM 3D printers have a critical issue of bending and swelling caused by the moisture in the ECM. Such undesired deformation of microchannels must be avoided in *in vitro* vascular models designed to investigate the relationship between mechanical stress and cellular response, as unexpected alterations from the designed stress distribution may arise due to geometric inaccuracy. Thus, there remained a challenge to be solved in the fabrication process: the deformation of the sacrificial template should be reduced as much as possible. Despite this critical issue, previous studies on sacrificial molding have rarely addressed the deformation of sacrificial templates.

To suppress the deformation of 3D-printed water-soluble materials in an ECM hydrogel, we propose groove-aided sacrificial molding (GAS molding), adding the step to stamp grooves to sacrificial molding with the support materials (Fig. 1). To prevent undesired deformation of the sacrificial template, an ECM layer with a groove was prepared using a groove template. Then, the sacrificial template was fitted into the groove and was subsequently encapsulated in the ECM. The template for the groove was fabricated using an FDM 3D printer as well as the sacrificial template. Owing to the groove on the sacrificial template, the shape retention of the sacrificial template was enhanced, and the undesired deformation of the sacrificial template was reduced. In this study, we used gelatin as the scaffold material, a hydrogel derived from collagen, the major structural component of the native ECM. We evaluated our GAS molding method by analyzing the fabricated TG-gelatin-based microchannels with

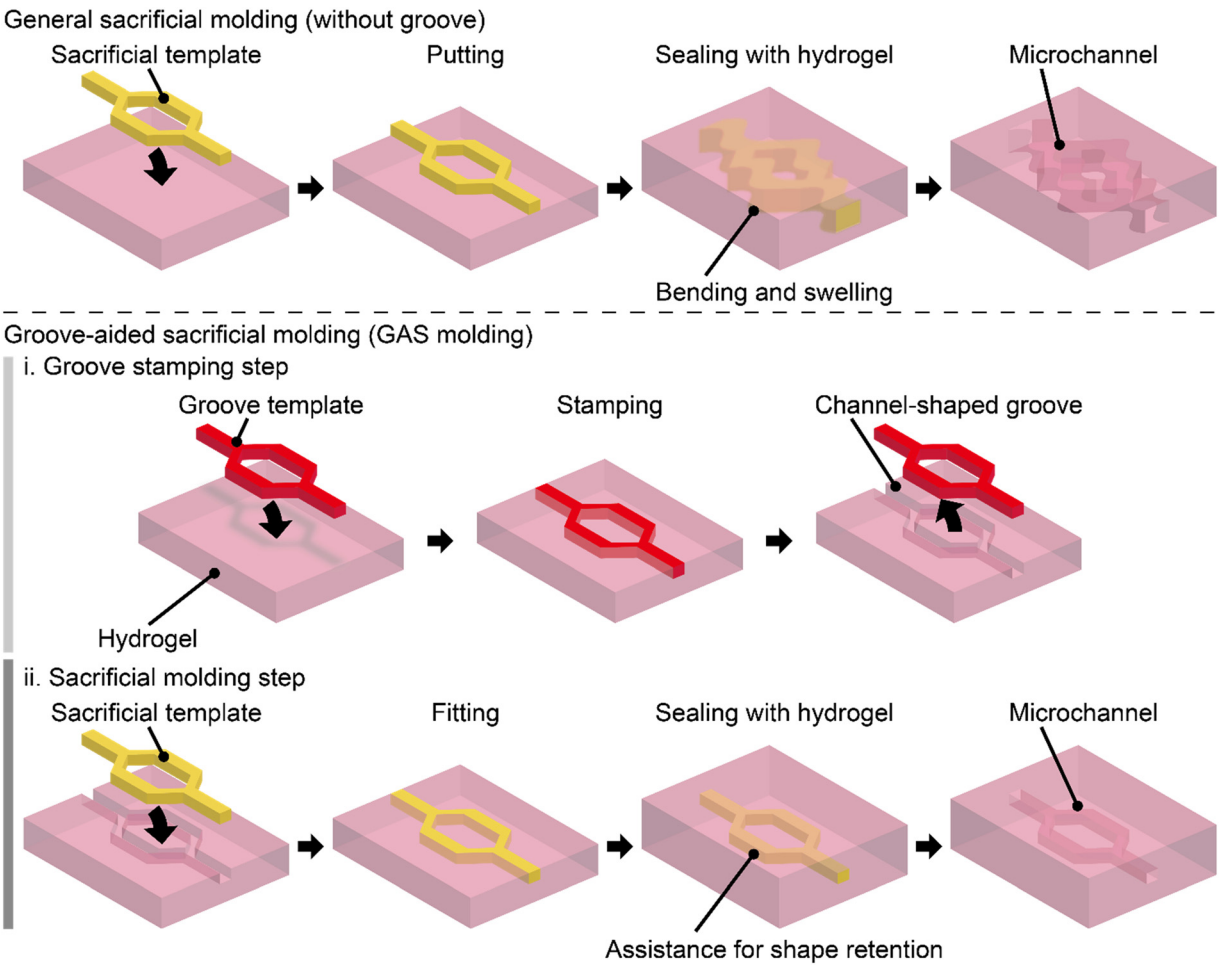

Fig. 1 Conceptual illustration of the groove-aided sacrificial molding (GAS molding). The fabrication process consists of a groove stamping step and a sacrificial molding step. The groove reduces the bending and swelling of the sacrificial template.

and without groove-aided processes. In addition, we tested the applicability of our fabricated branched *in vitro* vascular model to the construction of an *in vitro* vascular model for analyzing the response of the endothelial tissue to mechanical stretch and fluid shear stress. Finally, the presence of endothelial-function-related proteins in our *in vitro* vascular model was confirmed by immunofluorescence staining. Our demonstration suggests a platform to spatially elucidate the cellular responses to irregular mechanical stresses, such as triggers of cardiovascular disease.

Materials and methods

Preparation of gelatin pre-gel solutions

Phosphate buffered saline (10×) (−) (PBS (−), P5493, Sigma-Aldrich) was diluted 10 times with ultrapure water (hereinafter referred to as PBS). Gelatin powder (gelatin from porcine skin, G1890, Sigma-Aldrich) was dissolved in PBS at 45 °C to be 15% (w/v). The dissolved gelatin solution (gelatin pre-gel solution) was stored at 4 °C until use. To prepare the transglutaminase (TG) solution as a cross-linking agent for gelatin, TG powder (Moo Gloo TI Transglutaminase, 1203-50, modernist pantry) was dissolved in PBS at 45 °C to be 5% (w/v). The TG solution was stored at −20 °C until use.

Fabrication of templates using a 3D printer

3D models of the desired microchannel shape were designed using computer-aided design (CAD) software (Fusion 360, Autodesk) and exported in the standard triangulated language (STL) format. The STL files of the 3D models were imported into the slicer software (Qidi Print, Qidi Technology, and MakerBot Desktop, MakerBot) and exported as G-code files. The G-code files were uploaded to the FDM 3D printer (X-smart, Qidi Technology) to print the templates. For the groove template, polylactic acid (PLA, B08DLH82KY, Ankun), a standard material for FDM 3D printing, was selected. For the sacrificial template, PVA (101-90-142, SainSmart), a standard support material for FDM 3D printing, was selected. In this study, templates with three types of shape were designed: straight microchannels, Y-shaped microchannels (detailed in the section "Evaluation of microchannel dimensions and shapes"), and a branched microchannel for the vascular model (detailed in the section "Fabrication of a branched microchannel for the vascular model").

Fabrication of microchannel by GAS molding

The prepared gelatin pre-gel solution and TG solution were mixed at 45 °C to a volume ratio of 5 : 1. The printed groove template was placed on a dish (130181, BioLite), and the TG-gelatin mixture[33–35] (pre-gel solution) was poured using a syringe (SS-10SZ, TERUMO) (Fig. 2(a)). The pre-gel solution was cured by cooling at 4 °C for 10 min to form a TG-gelatin sheet with the groove. After the TG-gelatin sheet was flipped over, the groove template was removed (Fig. 2(b)). The printed sacrificial template was then fitted into the groove on the TG-gelatin sheet. After that, the pre-gel solution was poured again (Fig. 2(c)). The poured pre-gel solution was cross-linked by incubation at 37 °C for 2 h. The cross-linking of the TG and gelatin was stabilized by cooling at 4 °C for 12 h. The TG-gelatin containing the sacrificial template was cut to reveal both ends of the sacrificial template. Hot water was injected to dissolve the sacrificial template to form the branched microchannel in the TG-gelatin (Fig. 2(d)). In the case of fabricating microchannels by sacrificial molding (without using the groove) for comparison, steps (a) and (b) in Fig. 2 were skipped.

Evaluation of microchannel dimensions and shapes

Two designs of microchannels, straight and Y-shaped, were fabricated by sacrificial molding with and without the aid of the grooves, respectively, to evaluate the dimensions and

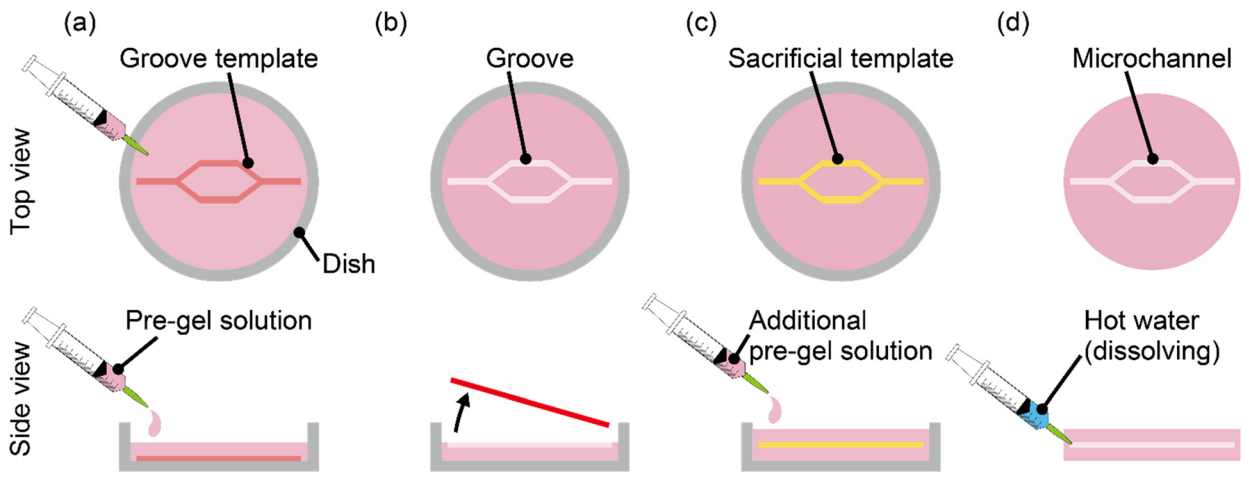

Fig. 2 Detailed process of the GAS molding. (a) Fabrication of the bottom layer with a groove. (b) The groove template is removed from the bottom layer. (c) Fabrication of the top layer with a sacrificial template. (d) The sacrificial template is dissolved in hot water after gelation.

shapes of the TG-gelatin microchannels. As for the straight microchannels (length = 30 mm), four types (with varying widths and heights) were designed: 1.0 mm × 1.0 mm, 0.8 mm × 0.8 mm, 0.6 mm × 6.0 mm, and 0.4 mm × 0.4 mm. As for the Y-shaped branched microchannels (length of each side = 15 mm), four types of branch angles were designed (30°, 60°, 90°, and 120°) with a width and height of 0.4 mm × 4.0 mm.

To visualize the shape of the fabricated microchannels, a 5% (w/v) gelatin solution (gelatin powder dissolved in PBS at 45 °C) containing 0.1% (v/v) green fluorescent microbeads (diameter: 0.2 μm, carboxylate-modified microspheres, F8811, Invitrogen) was introduced into the fabricated microchannels and cooled to 4 °C to solidify the gelatin solution. Segmented fluorescence images of the microchannels were taken using an inverted fluorescence/phase-contrast microscope (IX73PI-22FL/PH, EVIDENT). The segmented fluorescence images of the microchannels were tiled and combined. The combined images were processed with Fiji, a distribution of ImageJ (National Institutes of Health). Representative five points of the width of the straight microchannel were measured and averaged to define as a channel width. The combined images were converted to 8-bit grayscale and binarized. The binarized images were imported into the illustration software (Illustrator, Adobe) and outlined. For the straight microchannels, the edges of the microchannels with 20 mm lengths were extracted from the outline to measure the length and width of the bounding box of the microchannel. The aspect ratio of the bounding box was calculated and defined as distortion. For the Y-shaped microchannels, the angle of the microchannels at the branched point was measured.

Fabrication of a branched microchannel for the vascular model

A TG-gelatin-based microchannel with branches for perfusion and stretching culture was fabricated by GAS molding. The branched microchannel was designed to have four holes on each side parallel to the microchannel for stretching culture (Fig. 3(a)). For perfusion of the medium, silicone tubes (285-01778, Hagitec, and 9-869-04, LABORAN) were connected to the inlet and outlet of the microchannel. To fix the silicone tubes, a polydimethylsiloxane (PDMS, Silpot 184, Dow Corning Toray Co., Ltd.) frame was prepared. The branched microchannel was designed to have two generations of branching (Fig. 3(b)). In the first generation of the branch, the channel width split from 1.6 mm to 0.8 mm. In the second generation, the width split from 0.8 mm to 0.4 mm. The total cross-sectional area of the branched microchannel perpendicular to the flow direction was kept constant because the microchannel had a constant height of 0.4 mm. Therefore, the branched microchannel was designed to distribute a constant flow rate per cross-sectional area throughout the channel.

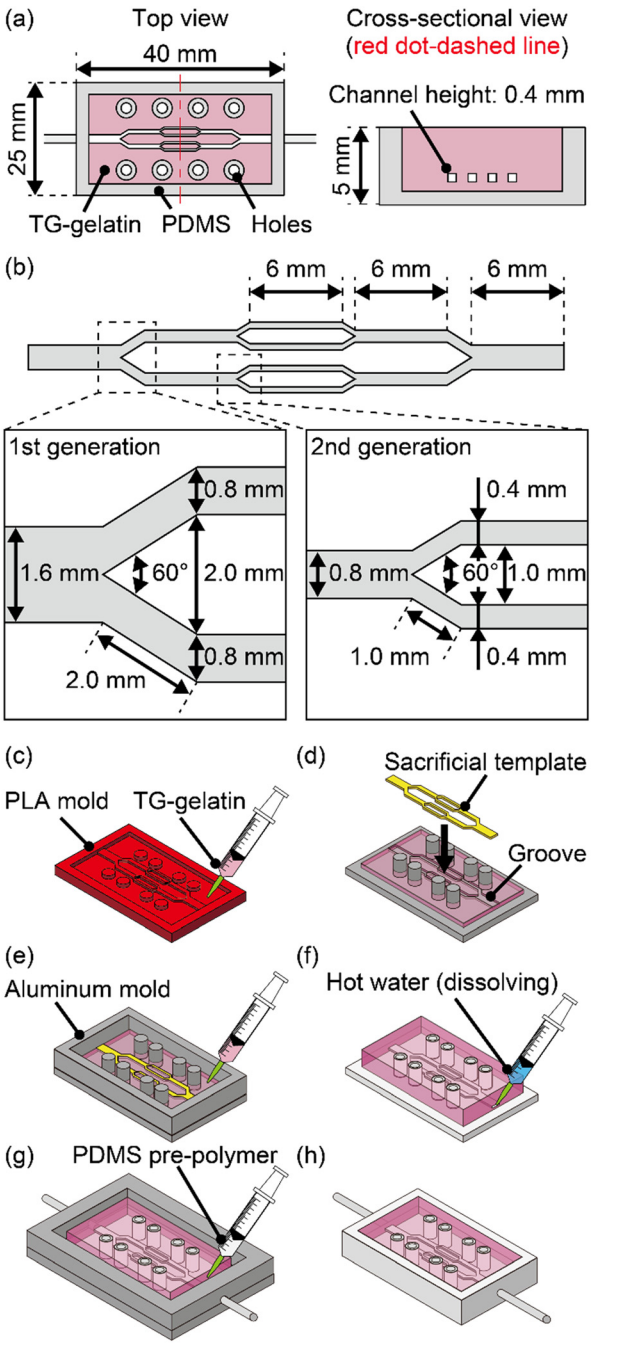

Fig. 3 The fabrication process of the branched microchannel for the *in vitro* vascular model. (a) The design of the branched microchannel. The microchannel consists of TG-gelatin and PDMS. (b) Dimensions of the branched microchannel. (c) Fabrication of the bottom layer with a groove. (d) The bottom layer and sacrificial template are set on an aluminum mold. (e) Fabrication of the top layer. (f) Dissolving the sacrificial template. (g) Fabrication of a PDMS frame. (h) Schematic image of the fabricated *in vitro* vascular model.

A PLA mold was printed by FDM 3D printing to stamp the channel-shaped groove onto the TG-gelatin sheet (Fig. 3(c)). The TG-gelatin pre-gel solution warmed to 45 °C was poured into the PLA mold. Then, the TG-gelatin solution was cooled at 4 °C for 10 min for curing. After curing, the TG-gelatin

sheet with the groove was flipped to set on an aluminum mold with pillars fabricated by machining (Fig. 3(d)). The 3D-printed sacrificial template was set into the groove. To encapsulate the sacrificial template, the TG-gelatin pre-gel solution was poured onto the sacrificial template surrounded by an aluminum frame (Fig. 3(e)). After incubation at 37 °C for 2 h, the crosslinked TG-gelatin scaffold was set on the prepared PDMS sheet with pillars (Fig. 3(f)). The sacrificial template was dissolved in hot water (95 °C) to form branched microchannels in the TG-gelatin scaffold. The TG-gelatin scaffold and PDMS sheet were set in an aluminum mold with silicone tubes (Fig. 3(g)). A PDMS pre-polymer solution mixed with a base polymer and curing agent at a ratio of 10 : 1 was poured around the TG-gelatin scaffold. After PDMS curing at 75 °C for 2 h, the TG-gelatin-based microchannel surrounded by a PDMS frame was fabricated (Fig. 3(h)).

Perfusion and stretching of the branched microchannel

The perfusion and stretching culture system was built with syringe pumps and motorized stages (detailed images are shown in Fig. S1). To stretch the branched microchannel, the branched microchannel was mounted on the perfusion and stretching culture system. The branched microchannel was stretched by 5% (= 0.55 mm) and 10% (= 1.1 mm). For visualizing perfused flow, green fluorescent microbeads with a diameter of 10 μm (carboxylate-modified microspheres, F8836, Invitrogen) were mixed in ultrapure water to be 1% (v/v). The fluorescent bead solution was perfused into the branched microchannel at a flow rate of 0.64 μL s^{-1} (= flow velocity of 1 mm s^{-1} in the branched microchannel). The flow of the fluorescent beads was recorded using an inverted fluorescence microscope under varied stretching conditions: no stretching, 5% stretch at 0.5 Hz, 5% stretch at 1.0 Hz, and 5% stretch at 2.0 Hz. The movement of the perfused fluorescent beads was traced using the motion analyzing software (VW-9000 Motion Analyzer, VW-H2MA, Keyence).

Cell culture

Human saphenous vein endothelial cells (HSaVECs, C-12231, PromoCell)[36,37] were cultured with the Endothelial Cell Growth Medium-2 BulletKit™ (EGM-2, CC-3162, Lonza) in a humidified atmosphere at 37 °C with 5% CO_2 to 80% confluence. For passaging, HSaVECs with passage numbers 5 to 7 were rinsed with PBS. For cell detachment, the HSaVECs were treated with 0.125% trypsin-EDTA (TE, 25200072, Thermo Fisher Scientific). After the detachment, the fresh medium was added to the trypsinized cells to prepare the cell suspension. The cell suspension was centrifuged at 300 *g* for 3 min at 22 °C to collect the cells. The pelleted cells were re-suspended in a fresh medium to seed into dishes. The cells were passaged several times before experiments to ensure stable proliferation.

Perfusion and stretching culture with the vascular model

The TG-gelatin-based microchannel with branches was soaked in ultrapure water to autoclave in a cycle of 20 min at 120 °C for sterilization. The autoclaved branched microchannel was placed in a 60 mm dish (130181, BioLite). Then, the branched microchannel was incubated with 5 mL of EGM-2 in a 37 °C culture incubator with 5% CO_2 (MCO-170AICUV, PHCbi) over 1 day. The HSaVEC suspension was prepared at a concentration of 1.0×10^7 cells per mL. After removing the EGM-2 around the branched microchannel, the HSaVEC suspension was injected into the branched microchannel using needles (NN-1838 N, Terumo) and plastic syringes (SS01T, Terumo). The branched microchannel filled with the cell suspension was incubated for 2 h in a culture incubator for adhesion of the HSaVECs to the TG-gelatin scaffold.

The UV-sterilized perfusion and stretching culture system was placed in the culture incubator. The perfusion tubes were autoclaved. For the preparation of the perfusion culture, the perfusion tubes and plastic syringes (SS-30ESZ, Terumo) were filled with EGM-2. The vascular model with HSaVECs was connected to the perfusion tubes. After the connection, the vascular model was mounted on the perfusion and stretching culture system. A 60 mm dish was set under the vascular model to soak the vascular model in EGM-2. The plastic syringes filled with EGM-2 were installed into the syringe pumps. Finally, HSaVECs were cultured in the vascular model under perfusion and stretching for 3 days. HSaVECs were cultured under the following two mechanical stress conditions: no stretching with 0.01 dynes per cm^2 (= 2.14 μL min^{-1}) and 5% 1.0 Hz stretching with 10 dynes per cm^2 (= 2.14 mL min^{-1}).

Finite element simulation of solid and fluid mechanics

TG-gelatin cubes (5 mm per side) were fabricated. Young's moduli of the cubes were measured using our previously reported method.[38,39] The density of TG-gelatin was calculated by measuring the mass of TG-gelatin pre-gel solution per 1 mL. The Poisson's ratio of TG-gelatin was set to 0.49, assuming incompressible material behavior. A CAD model of the branching part in the vascular model was designed using Fusion 360. The CAD model was imported into the finite element method software (COMSOL Multiphysics software, COMSOL, Inc.) using the CAD import module. The material properties of TG-gelatin were set for the scaffold, and the properties of the perfused fluid were set as standard water. Prescribed displacements and velocities were set on both sides of the simulation model to achieve a stretch amount of 5% and frequencies of 1 Hz. The flow velocity was set at the inlet of the microchannel based on the flow rates used in the experiment (2.14 mL min^{-1}), and the outlets were set at 0 Pa. A normal-sized mesh was generated for time-dependent analysis. Von Mises stress derived from cyclic stretching and fluid shear stress derived from medium perfusion were simulated using the structural mechanics

module and laminar flow module, respectively. Three points were set within the branched microchannel for plotting, and a graph of the change in flow velocity was plotted. The stress distribution along the inner walls of the branched microchannel was visualized using a cross-sectional clipping function.

Immunofluorescence staining

PECAM1 (an endothelial cell adhesion molecule and mechanoreceptor[40,41]), integrin α9 (one type of integrin family that is a mechanoreceptor[42,43]), actin filaments (the cytoskeleton), and cell nuclei were fluorescently stained. To fix the HSaVECs in the vascular model, a 4% paraformaldehyde phosphate-buffered solution (PFA, 163-20145, Wako) at 37 °C was perfused into the vascular model at a flow rate of 50 μL min^{-1} for 20 min (hereafter, unless otherwise described, the flow rate of the solution is 50 μL min^{-1}). After that, PBS was perfused for 15 min to rinse the vascular model. 0.2% (v/v) Triton X-100 (A16046, Thermo Fisher Scientific) in PBS was perfused for 5 min to permeabilize the HSaVECs. PBS was then perfused for 15 min to rinse the vascular model. 5% (w/v) bovine serum albumin (BSA, A2153-10G, Sigma-Aldrich) in PBS was perfused for 20 min for blocking treatment. The primary antibodies for PECAM1 (BBA7, R&D Systems) and for integrin α9 (NBP2-16972, Novus Biologicals) were diluted in 5% BSA to a volume ratio of 1 : 1 : 400. The solution of the primary antibodies was perfused for 5 min. Then, the vascular model was incubated at 4 °C overnight. After the primary antibody

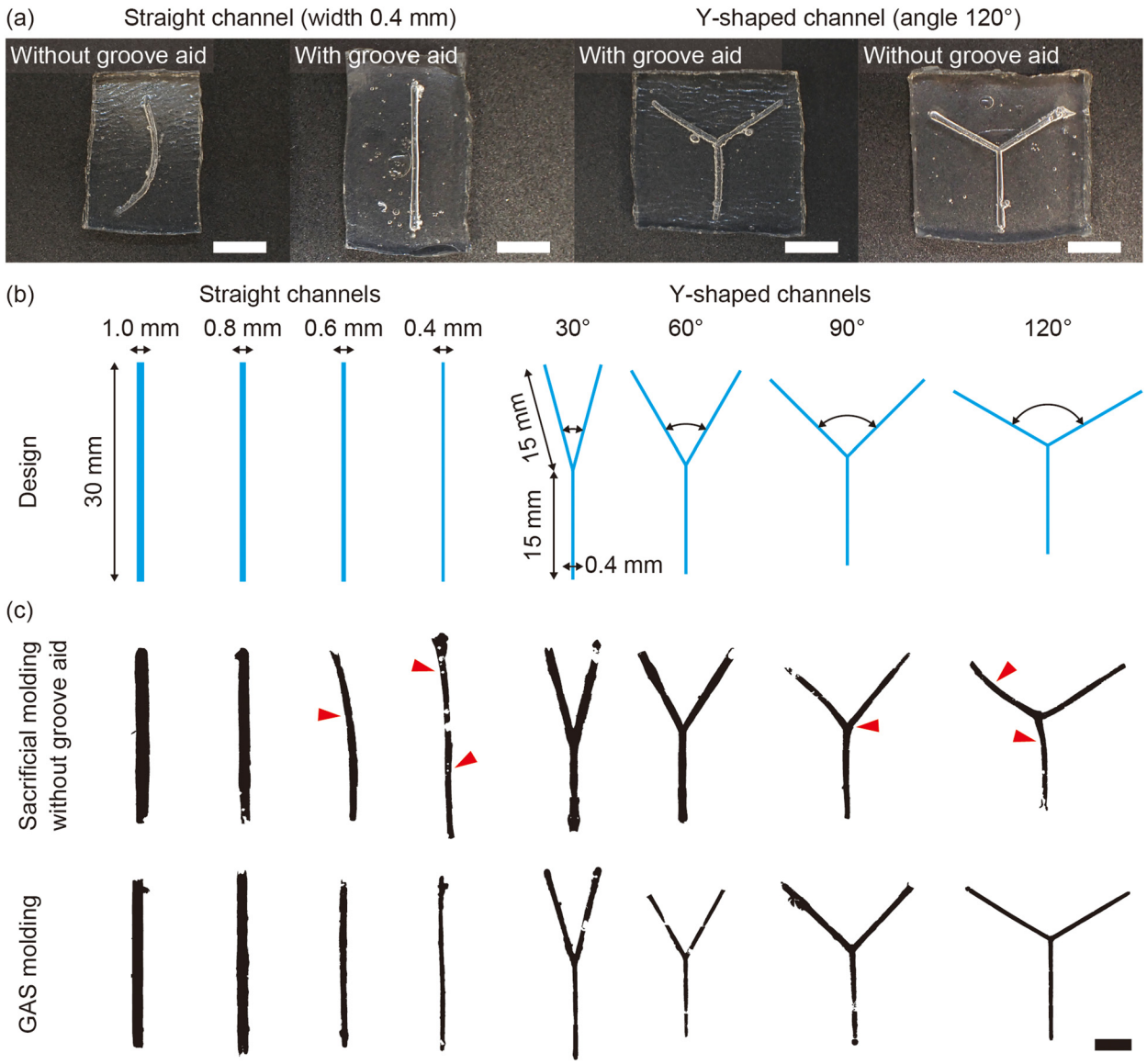

Fig. 4 (a) Fabricated TG-gelatin-based microchannels by sacrificial molding without groove aid and GAS molding. (b) Graphical designs of straight microchannels and Y-shaped microchannels. (c) Binarized images of microchannels fabricated by sacrificial molding without groove aid and GAS molding. The red triangles highlight the bends of the microchannels. Scale bars are 10 mm for (a) and 5 mm for (c).

reaction, PBS was perfused for 15 min to rinse the vascular model. The secondary antibodies (anti-mouse immunoglobulin G (IgG)-Alexa Fluor™ 568, A11004, Thermo Fisher Scientific, and anti-rabbit IgG-Alexa™ Fluor 647, A32733, Thermo Fisher Scientific) were diluted in 5% BSA to a volume ratio of 1 : 1 : 200. The secondary antibodies solution was perfused for 5 min. Then, the vascular model was incubated at room temperature for 1 hour. After the secondary antibody reaction, PBS was perfused for 20 min to rinse the vascular model. The 4′,6-diamidino-2-phenylindole (DAPI, D1306, Invitrogen) was diluted in PBS to a volume ratio of 1 : 1000. The DAPI solution was perfused for 5 min. PBS was perfused for 20 min to rinse the vascular model. To fix HSaVECs, 4% PFA was perfused into the vascular model for 20 min. PBS was perfused for 10 min to rinse the vascular model. After fluorescence staining, the aqueous-based mounting medium (Fluoromount/Plus, K048, Diagnostic BioSystems) was dropped into the inlet and outlet of the microchannels to prevent fluorescence fading. The stained HsaVECs in the vascular model were observed using a confocal laser scanning microscope (FV3000, EVIDENT).

Results and discussion

Evaluation of microchannel dimensions and shapes

To study the difference in the deformation of the fabricated channel shape *via* sacrificial molding with and without grooves, TG-gelatin-based microchannels were fabricated (Fig. 4(a)). Four types of straight channels and four types of Y-shaped channels were designed for the evaluation of deformation, respectively (Fig. 4(b)). To take images of the channel shape, the fabricated microchannels were filled with a solution containing fluorescent beads. The fluorescence images of the microchannels were binarized to measure the channel width, distortion, and angle (Fig. 4(c)). Comparing the cases with and without groove aid, the microchannels fabricated by sacrificial molding without grooves were more distorted than with grooves, especially in straight channels with 0.6 mm and 0.4 mm width and Y-shaped channels with 90° and 120° (highlighted by the red triangle in Fig. 4(c)).

To quantify the deformations, the channel width, distortion, and angle were measured using Fiji ImageJ (Fig. 5). The channel width was measured to evaluate channel swelling (Fig. 5(a), left). The distortion and angle were measured to evaluate channel bending (Fig. 5(a), center and right). The microchannels fabricated by sacrificial molding without grooves were around twice as wide as designed (swelling rate of the sacrificial molding without grooves: 191.9 ± 19.9%, n = 4, mean ± S.D.), whereas the GAS molding reduced the channel width to around 1.5 times (swelling rate of the GAS molding: 156.9 ± 6.5%, n = 4, mean ± S.D., Fig. 5(b)). Thus, the groove GAS molding assisted in reducing the deformation of the channel width due to the swelling of the sacrificial template. In addition, the microchannels fabricated by GAS molding showed lower distortion than those by sacrificial molding for all channel designs (distortion of the sacrificial molding without grooves: 2.53 ± 0.64%, n = 4, mean ± S.D., and GAS molding: 1.43 ±

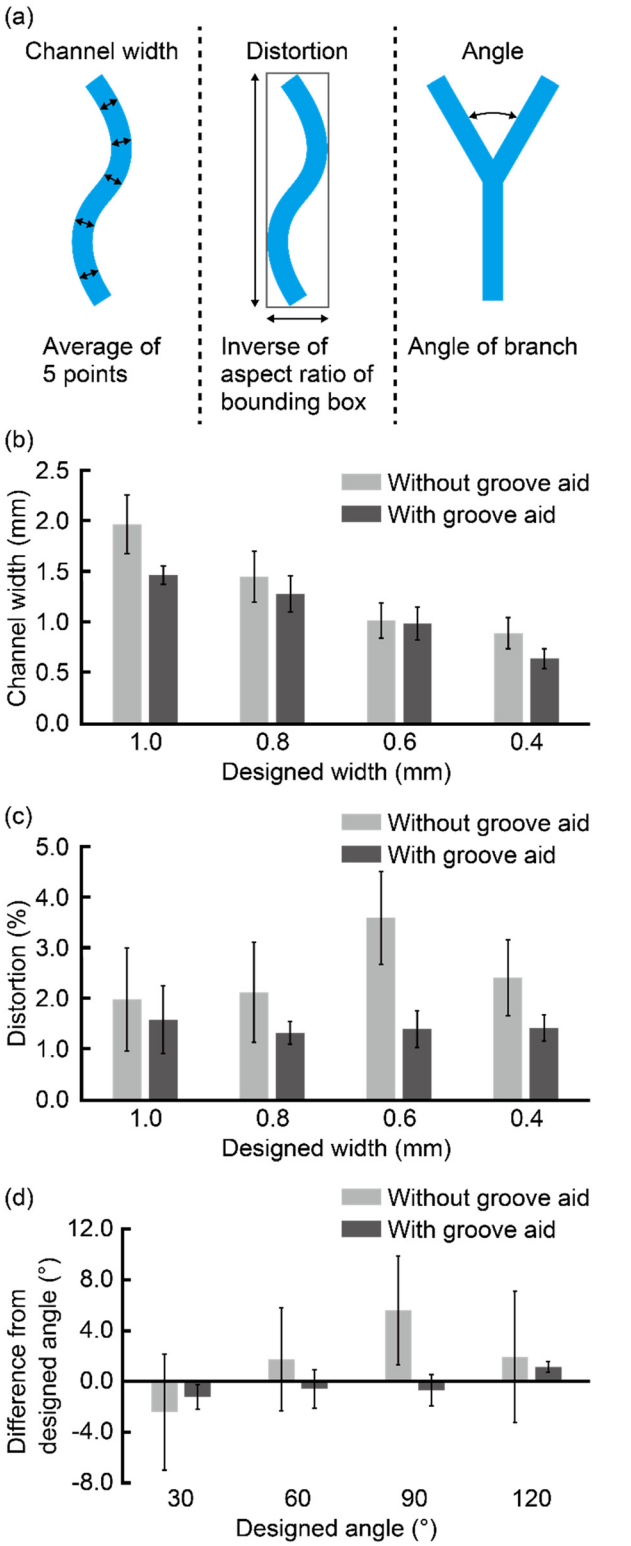

Fig. 5 Graphs of the measured dimensions of the microchannels. (a) Evaluation indicators of microchannel dimensions. (b) Measured channel width. (c) Calculated distortion. (d) Calculated difference from a designed angle in the Y-shaped channels. Data are represented as mean ± S.D. The number of samples is n = 5.

0.09%, n = 4, mean ± S.D.), indicating that the groove in the GAS molding could also work to prevent the bending of the sacrificial templates compared to the sacrificial molding without a groove (Fig. 5(c)).

The error bars represent the standard deviation of the repeated measurement (Fig. 5(b and c)), indicating that the variation of the measured channel widths and the distortion were smaller in the sacrificial molding with grooves than without grooves for all channel designs. This observation suggested that the groove in the GAS molding inhibits swelling and bending of the sacrificial template and helped precisely fabricate microchannels with desired shapes and dimensions.

Lastly, the measured angles fabricated by GAS molding were closer to the designed angles than those fabricated without the aid of grooves (absolute value of difference from the designed angle of the sacrificial molding without grooves: 1.70 ± 2.83°, n = 4, mean ± S.D., and GAS molding: 0.34 ± 0.89°, n = 4, mean ± S.D.) (Fig. 5(d)). The standard deviations were also smaller in the GAS molding (average of standard deviation: 1.04°) than in the sacrificial molding without a groove (average of standard deviation: 3.61°). This observation suggested that the GAS molding was also practical in fabricating branched microchannels with desired branch angles. In summary, our results suggested that GAS molding is more effective in fabricating narrow and branched microchannels than sacrificial molding without grooves.

Perfusion and stretching of the branched microchannel

To demonstrate that the fabricated microchannel by GAS molding was stable during stretching and perfusion culture,

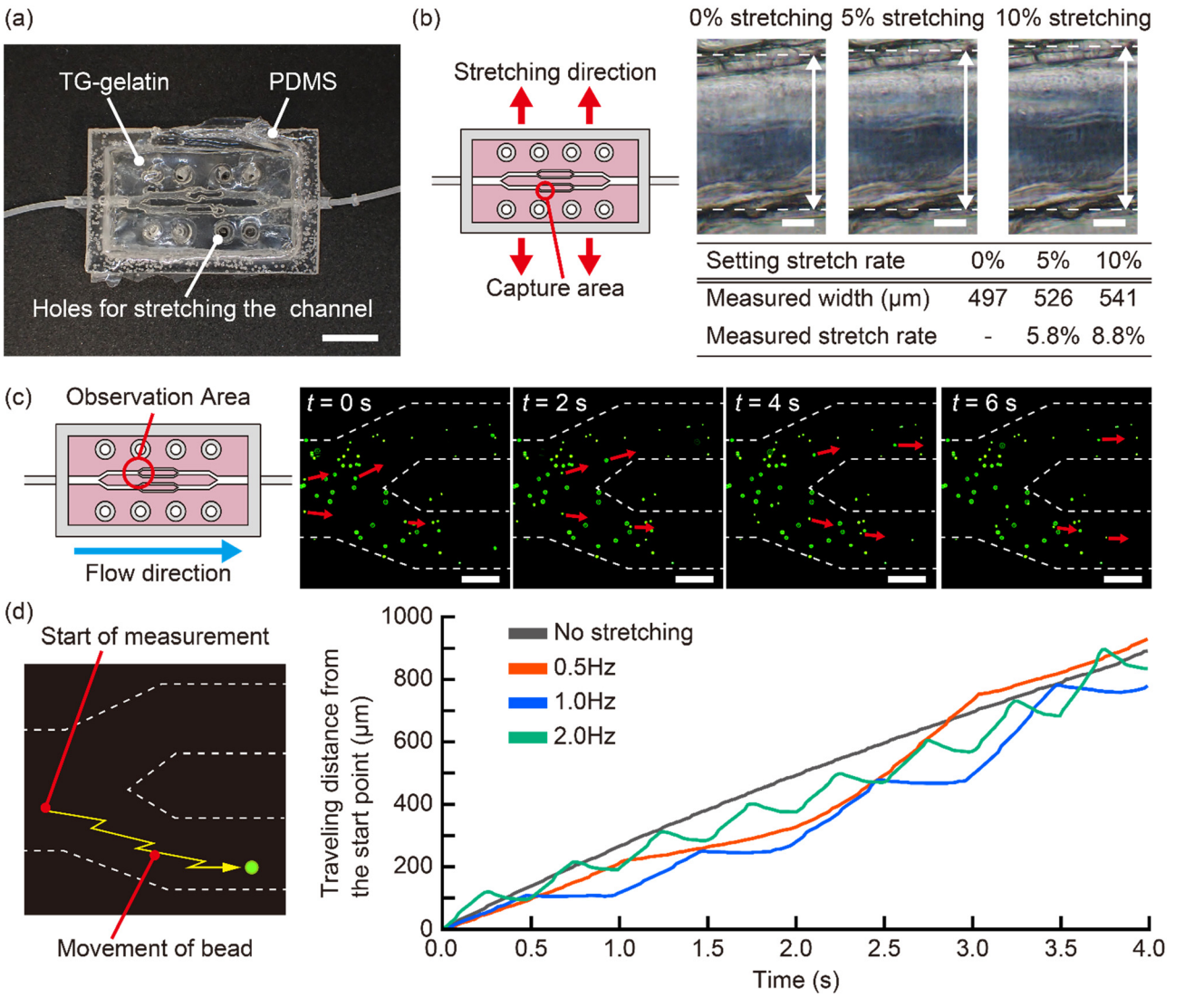

Fig. 6 (a) TG-gelatin-based microchannel with branches fabricated by GAS molding. A PDMS frame surrounds microchannels with TG-gelatin scaffolds. (b) Phase-contrast images of the microchannel under stretching. (c) Split images of perfusing fluorescent beads into the branched microchannel under no stretching. (d) Graph of the distance travelled by fluorescent beads from the start position. Scale bar is 10 mm for (a), and scale bars are 100 μm for (b), and scale bars are 500 μm for (c).

the branched microchannel was tested with the perfusion and stretching culture system (Fig. S1). First, a TG-gelatin-based microchannel with branches (detailed design shown in Fig. 3(a) and (b)) was fabricated by GAS molding (Fig. 6(a)). Several holes were designed around the TG-gelatin-based microchannel for connection to the stretching stage. Then, the branched microchannel could be mounted on the perfusion and stretching culture system (Fig. S1(d)).

To observe the stretching of the microchannels, the TG-gelatin-based microchannel was stretched with the perfusion and stretching culture system (Fig. 6(b)). The branched microchannel was stretched by 10% without breaking. Thus, the TG-gelatin-based microchannel had sufficient strength to withstand mechanical stress to this strain. The channel width was 497 μm without stretch, 526 μm under 5% stretching (= 5.8% extension compared to no stretching), and 541 μm under 10% stretching (= 8.8% extension to no stretching).

Next, to test the perfusion capability of the fabricated microchannel during the stretching, the fluid flow in the branched microchannel was visualized. The fluorescent bead-suspended solution was perfused into the microchannel fixed on the perfusion and stretching culture system at a flow rate of 0.64 μL s^{-1} (movies of bead flow are shown in Movies S1–S4). The movement of the fluorescent beads at the branched area under no stretching was traced for 6 seconds (Fig. 6(c)).

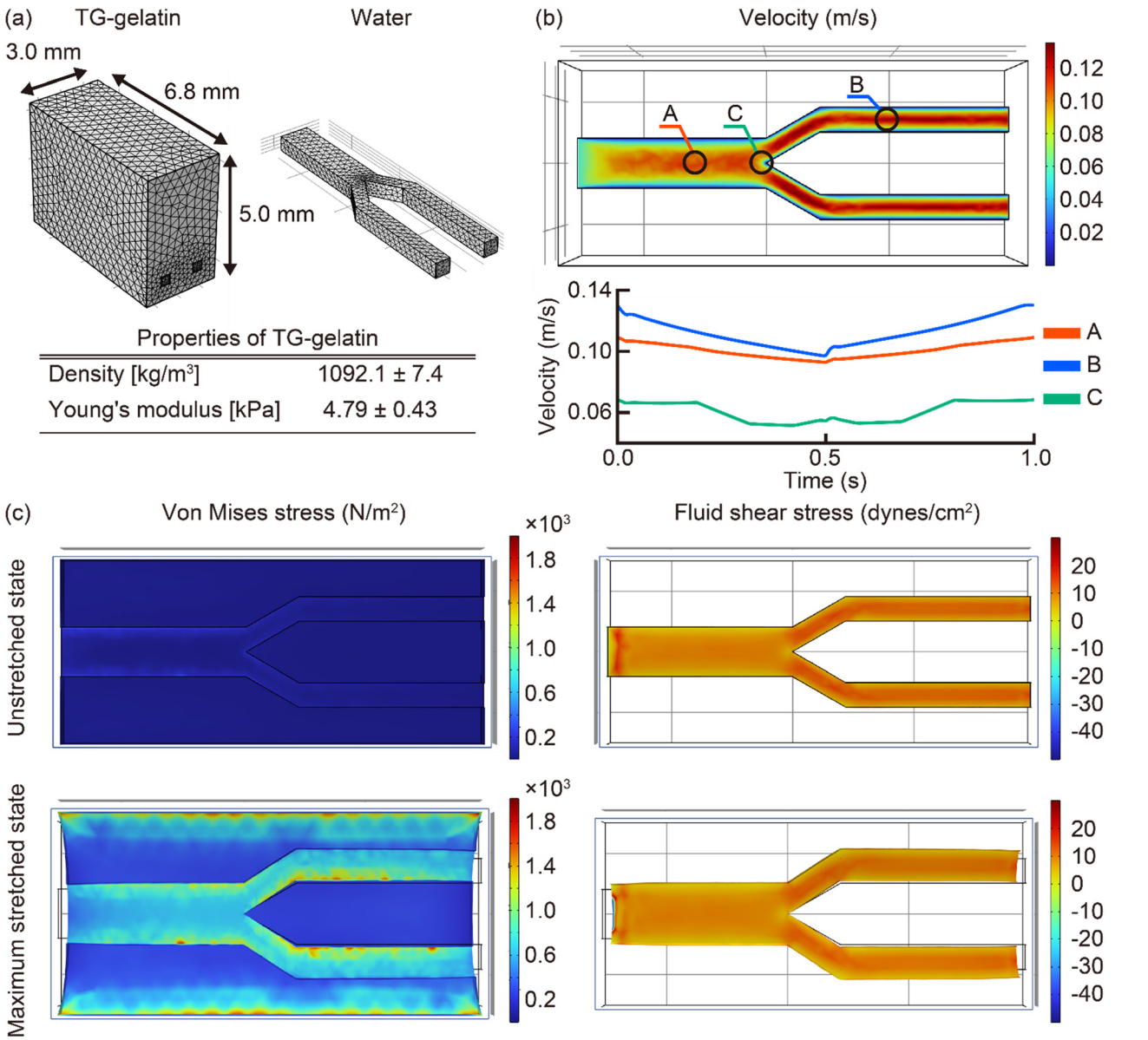

Fig. 7 (a) Mesh models generated in COMSOL. The material properties of TG-gelatin were represented as mean ± S.D. The number of samples is n = 3. (b) A scalar map of flow velocity on the mid-height plane of the branched microchannel. The graph shows temporal changes in flow velocity during one cycle of stretching at three points. (c) The distributions of von Mises stress and the fluid shear stress on the inner wall in stretched and unstretched states.

The flow of fluorescent beads was divided into two directions, meaning that liquid in the branched microchannel was perfused through the whole microchannel. Furthermore, cyclic stretching (5%, 0.5–2.0 Hz) was conducted together with the perfusion. The motion of the fluorescent beads in the microchannel oscillated, responding to the stretching cycle, indicating that the perfusion and stretching culture system generated a pulsatile flow in the microchannel. Discussing the relationship between the frequency of stretching and movement of beads, the beads constantly flowed forward at 0.5 Hz, and repeatedly flowed forward and stopped at 1.0 Hz, and repeatedly flowed forward and backwards at 2.0 Hz (Fig. 6(d)). These results indicated that our perfusion and stretching culture system could offer several types of pulsatile flow, which would be essential to mimic blood flow *in vivo*.[44,45]

Finite element simulation of solid and fluid mechanics

To quantitatively estimate the flow velocity, von Mises stress, and fluid shear stress changes within the branched microchannel, COMSOL simulations were performed under stretching and perfusion conditions. A standard-sized mesh model was generated for a clipped model of the branched microchannel (Fig. 7(a)). The material properties of TG-gelatin were determined through experiments measuring Young's modulus and density (density: 1092.1 ± 7.4 kg m^{-3}, n = 3, mean ± S.D., and Young's modulus: 4.79 ± 0.43 kPa, n = 3, mean ± S.D.).

A scalar map of flow velocity was plotted with a color scale on the mid-height plane of the branched microchannel (Fig. 7(b)). Temporal changes in flow velocity during one cycle of stretching were visualized as graphs at three points: before the branching (point A), after the branching (point B), and at the branching (point C). From 0.0 to 0.5 s, the model was stretched, and from 0.5 to 1.0 s, it returned to its original state. In the straight areas (points A and B), the velocity reached a minimum at 0.5 s, indicating a pulsatile flow pattern like a triangular wave. Interestingly, at the branching point (point C), the velocity slightly increased around 0.5 s, forming a pulsatile flow with troughs at approximately 0.42 s and 0.58 s. These results quantitatively demonstrate the heterogeneous temporal velocity changes in the branched microchannel under complex mechanical stimuli, as simulated by COMSOL. The combination of tracer particle tracking experiments and fluid dynamic simulations enables detailed analysis of complex fluid behavior under mechanical conditions that are difficult to understand theoretically.

In addition, the von Mises stress from cyclic stretching and the fluid shear stress from medium perfusion on the inner wall of the *in vitro* vascular model were also estimated (Fig. 7(c)). The von Mises stress at the bottom surface of the microchannel ranged from 0.3 to 0.9 N m^{-2} in the unstretched state and increased to approximately 730 to 760 N m^{-2} in the maximum stretched state. A few local high-stress spots near the edge of the channel reached around 1800 N m^{-2}. On the other hand, the fluid shear stress showed little difference between the two stretch states, remaining around 10 dynes per cm^2. According to the velocity plots in Fig. 7(b), the maximum and minimum velocities were 0.11 m s^{-1} and 0.09 m s^{-1} at point A and 0.13 m s^{-1} and 0.10 m s^{-1} at point B, respectively. These data indicate that the stretching and perfusion culture conditions used in this study did not induce significant cyclic changes in fluid shear stress. Furthermore, the time-dependent stress variations were visually supported by Movies S5 and S6. Taken together, these results demonstrate that finite element simulation is a valuable approach for quantitatively analyzing the mechanical microenvironment in branched *in vitro* vascular models.

Perfusion and stretching culture with the vascular model

To show that vascular endothelial cells can be cultured under mechanical stress in the TG-gelatin-based microchannel fabricated by GAS molding, HSaVECs were cultured under perfusion and stretching. The *in vitro* vascular model fabricated by GAS molding remained structurally stable during perfusion and stretching culture (Fig. S2). After 3 days of perfusion and stretching culture (5% 1.0 Hz stretching with 10 dynes per m^2), nuclei and PECAM1 were stained by immunofluorescence staining (Fig. 8(a)). The phase-contrast image and immunofluorescence image show that HSaVECs were confluently organized on the inner wall of the TG-gelatin-based microchannel. Furthermore, a network structure of PECAM1, an intercellular adhesion molecule, was constructed over the entire surface. Therefore, the results indicated that HSaVECs maintained their organization without breaking under mechanical stress.

To compare the effects of mechanical stress on protein expression, DAPI, PECAM1, and integrin α9 were fluorescently stained throughout the whole branched microchannel (Fig. 8(b)). Then, to observe the distribution of protein expression, the branching region is presented in Fig. 8(c). Under both conditions, the network structure of PECAM1 was formed following the microchannel. On the other hand, focusing on the expression of integrin α9, integrin α9 was not activated under no mechanical stress (the green background in the image is due to elevated detector gain settings, and no distinct dot-like integrin α9 signal was observed). However, the distribution of integrin α9 was visualized under mechanical stress. Since integrin α9 has been reported to be elevated by flow stimulation,[46] this visualized distribution would reflect the distribution of upregulated integrin α9 by mechanical stress. Interestingly, although PECAM1 is also a mechanoreceptor, there is no remarkable difference in the distribution of PECAM1 expression with or without mechanical stress. Thus, the distribution of integrin α9 could capture mechanical stresses that PECAM1 does not detect. Notably, the *in vivo* vascular branches produce irregular changes in blood flow, including reverse and oscillatory flow. To examine cellular interactions

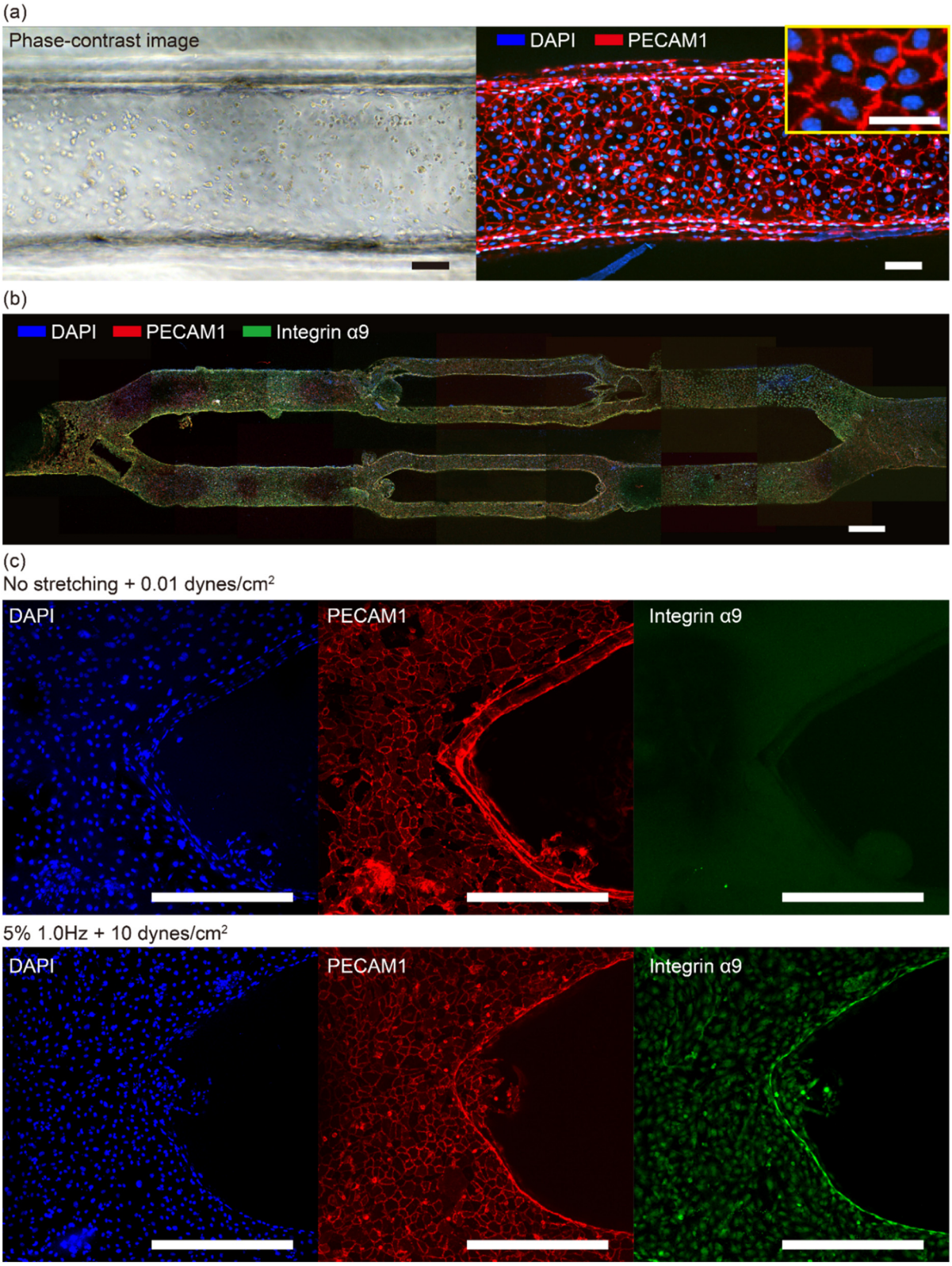

Fig. 8 (a) HSaVECs in the vascular model after 3 days of perfusion and stretching culture. (b) Macroscopic distribution of DAPI, PECAM1, and integrin α9 in the vascular model after 3 days of perfusion and stretching culture. (c) Detailed distribution of DAPI, PECAM1, and integrin α9 at the branched area with and without mechanical stress. Scale bars are 100 μm for (a) (50 μm in the detailed image), and scale bar is 1 mm for (b), and scale bars are 500 μm for (c).

with such irregular flows, the distribution of cellular responses related to the intensity of irregular mechanical stress would be analyzed by the two aspects of PECAM1 and integrin α9. In summary, the *in vitro* vascular model designed by GAS molding has validity as a tool for analyzing cellular responses to complex mechanical stresses.

Discussion

We proposed GAS molding as a method to fabricate TG-gelatin-based microchannels. Compared to general sacrificial molding without grooves,[29–32] the GAS molding could reduce the distortion of the sacrificial template due to moisture in the hydrogel scaffold. Therefore, adding the step of shape aid with grooves effectively reduced the deformation of the water-soluble sacrificial template. In addition, a TG-gelatin-based *in vitro* vascular model was designed to show the efficacy of the GAS molding. The vascular model composed of TG-gelatin and PDMS allowed vascular endothelial cells to be cultured under stretching and perfusion. Thus, the system proposed in this paper has the potential to be a platform for the analysis of cellular responses to complex mechanical stresses such as triggers of cardiovascular disease.

The rate of swelling of microchannels fabricated by GAS molding is critical in achieving the desired shape and dimension of the channel. Although the GAS molding was effective in reducing the bending of the sacrificial template, the swelling of the sacrificial template has not been entirely suppressed. To solve this issue, dimensional modification with correction values would be applied to GAS molding compared to sacrificial molding without a groove. The GAS molding showed a stable 1.5 times swelling of the microchannel under all conditions (Fig. 5(b), swelling rate of the GAS molding: 156.9 ± 6.5%, n = 4, mean ± S.D.). On the other hand, the sacrificial molding without a groove was unstable around twice the swelling (swelling rate of the sacrificial molding without grooves: 191.9 ± 19.9%, n = 4, mean ± S.D.). To summarize, the microchannels swell unstably depending on the channel width by sacrificial molding without grooves, while the microchannels swell stably by 1.5 times by GAS molding. Therefore, dimensional modification with correction values such as lithographic drawing[47–49] could be applied for the GAS molding. The issue of channel width swelling would be solved by preparing a design with a width correction of 66% to the ideal dimensions. In addition, the swelling of channel width may also be caused by the exposure time to moisture during the sol–gel transition of the TG-gelatin. Therefore, accelerating the gelling speed of the TG-gelatin is expected to improve the dimensional stability further. It has been reported that the gelling time of TG-gelatin shortens with increasing concentrations of both gelatin and transglutaminase.[50] Accordingly, optimization of these concentrations could serve as an alternative strategy to mitigate channel swelling.

When performing sacrificial molding using FDM-printed molds, the microchannel design is governed by the ability of the 3D printer. In this paper, the minimum channel width was designed as 0.4 mm since an FDM 3D printer with a 0.4 mm diameter nozzle was used. Commercially, nozzles with a diameter of 0.2–0.25 mm (ref. 51 and 52) are widely available to create filaments with fine line widths. Custom-made nozzles allowed for fabricating 0.1 mm line widths.[53] Considering the swelling rate of the GAS molding, the GAS molding could suggest the branched microchannel with a minimum width of 150 μm. This indicates a potential advantage of the GAS molding in terms of resolution, as previously reported branched vascular models fabricated by extrusion-based bioprinting typically have a minimum channel width of approximately 0.5 mm.[54,55] Regarding the classification of human blood vessels, their diameters range from 10–20 μm for capillaries, 30–1000 μm for arterioles and venules, 1–6 mm for arteries and veins, and 6–30 mm for aortas and venae cavae.[56,57] Therefore, GAS molding is suitable for mimicking blood vessels on scales larger than arterioles and venules. In the future, the developed method would allow *in vitro* capillary models to be freely designed by the development of FDM 3D printing technology.

Through correction of swelling and improvement of FDM 3D printing technology, the microchannel fabricated by GAS molding would be widely applied as culture chips to examine the relationship between mechanical stress and endothelial cells. The unique mechanical stresses specific to the *in vivo* vascular environment are hinged on disturbed blood flow dependent on random branches and diameter changes of blood vessels. Thanks to the GAS molding being based on a 3D printing technology, the GAS molding allows for flexible modification of microchannels, for example, the same design as the curvature and branches of the patient's blood vessels. In such cases, finite element analysis methods such as fluid dynamics and mechanical deformation could be helpful to consider the irregular distribution of mechanical stresses. Previous research has been proposed to simulate blood flow to elucidate the pathology of vascular diseases.[58,59] Thus, combining with such simulations, our vascular model would be able to spatially process the effects of mechanical stress on endothelial cells at the microscale. Our method would suggest a platform to elucidate the impact of mechanical stress on cardiovascular disease by combining biological cellular assays and engineered vascular models.

Conclusions

We proposed groove-aided sacrificial molding (GAS molding) to fabricate a TG-gelatin-based *in vitro* vascular model with branches. To compare the deformation of microchannels fabricated by sacrificial molding with and without grooves, straight and Y-shaped TG-gelatin-based microchannels were fabricated. GAS molding reduced width deformation (191.9 ± 19.9% to 156.9 ± 6.5%), distortion (2.53 ± 0.64% to 1.43 ± 0.09%), and angular difference from the designed angle (1.70 ± 2.83° to 0.34 ± 0.89°) compared to sacrificial molding without grooves. For the cell culture of the vascular model

under mechanical stress, the vascular model fabricated by GAS molding was stretched and perfused by a perfusion and stretching culture system. Fluorescent bead tracing indicated a unique pulsatile flow through the entire vascular model under stretching and perfusion. As a demonstration, HSaVECs were cultured in the vascular model under 5% 1.0 Hz stretching with 10 dynes per cm^2. The effects of mechanical stress in uniquely shaped areas were visualized by immunofluorescence staining of PECAM1 and integrin α9. Overall, our method would suggest a platform to spatially elucidate the cellular responses to irregular mechanical stresses, such as triggers of cardiovascular disease.

Conflicts of interest

There are no conflicts to declare.

Data availability

The data supporting this article have been included as part of the SI.

Supplementary information is available: The SI includes the components of the system used for perfusion and stretching culture, as well as phase-contrast images demonstrating the stability of the *in vitro* vascular model under stretching. See DOI: **https://doi.org/10.1039/D5LC00214A**.

Acknowledgements

This work was partly supported by Grant-in Aid for Scientific Research (B) (19H04440) from Japan Society for the Promotion of Science (JSPS), Japan, and JKA and its promotion funds from KEIRIN RACE, and the Ministry of Education (MOE), Singapore, for the project funding (MOE-T2EP50122-0025).

References

1 S. Kaptoge, L. Pennells, D. De Bacquer, M. T. Cooney, M. Kavousi, G. Stevens, L. M. Riley, S. Savin, T. Khan, S. Altay, P. Amouyel, G. Assmann, S. Bell, Y. Ben-Shlomo, L. Berkman, J. W. Beulens, C. Björkelund, M. Blaha, D. G. Blazer, T. Bolton, R. B. Beaglehole, H. Brenner, E. J. Brunner, E. Casiglia, P. Chamnan, Y. H. Choi, R. Chowdry, S. Coady, C. J. Crespo, M. Cushman, G. R. Dagenais, R. B. D'Agostino, M. Daimon, K. W. Davidson, G. Engström, I. Ford, J. Gallacher, R. T. Gansevoort, T. A. Gaziano, S. Giampaoli, G. Grandits, S. Grimsgaard, D. E. Grobbee, V. Gudnason, Q. Guo, H. Tolonen, S. Humphries, H. Iso, J. W. Jukema, J. Kauhanen, A. P. Kengne, D. Khalili, W. Koenig, D. Kromhout, H. Krumholz, T. H. Lam, G. Laughlin, A. Marín Ibañez, T. W. Meade, K. G. M. Moons, P. J. Nietert, T. Ninomiya, B. G. Nordestgaard, C. O'Donnell, L. Palmieri, A. Patel, P. Perel, J. F. Price, R. Providencia, P. M. Ridker, B. Rodriguez, A. Rosengren, R. Roussel, M. Sakurai, V. Salomaa, S. Sato, B. Schöttker, N. Shara, J. E. Shaw, H. C. Shin, L. A. Simons, E. Sofianopoulou, J. Sundström, H. Völzke, R. B. Wallace, N. J. Wareham, P. Willeit, D. Wood, A. Wood, D. Zhao, M. Woodward, G. Danaei, G. Roth, S. Mendis, O. Onuma, C. Varghese, M. Ezzati, I. Graham, R. Jackson, J. Danesh and E. Di Angelantonio, *Lancet Global Health*, 2019, **7**, e1332–e1345.
2 K. E. Cosselman, A. Navas-Acien and J. D. Kaufman, *Nat. Rev. Cardiol.*, 2015, **12**(11), 627–642.
3 D. A. Chistiakov, A. N. Orekhov and Y. V. Bobryshev, *Acta Physiol.*, 2017, **219**, 382–408.
4 E. Roux, P. Bougaran, P. Dufourcq and T. Couffinhal, *Front. Physiol.*, 2020, **11**, 533349.
5 R. G. Mannino, A. N. Santiago-Miranda, P. Pradhan, Y. Qiu, J. C. Mejias, S. S. Neelapu, K. Roy and W. A. Lam, *Lab Chip*, 2017, **17**, 407–414.
6 V. L. Silvestri, E. Henriet, R. M. Linville, A. D. Wong, P. C. Searson and A. J. Ewald, *Cancer Res.*, 2020, **80**, 4288–4301.
7 N. Mori, Y. Morimoto and S. Takeuchi, *Biofabrication*, 2019, **11**, 11001.
8 T. W. Secomb, *Annu. Rev. Fluid Mech.*, 2017, **49**, 443–461.
9 M. Potente and T. Mäkinen, *Nat. Rev. Mol. Cell Biol.*, 2017, **18**(8), 477–494.
10 F. Tovar-Lopez, P. Thurgood, C. Gilliam, N. Nguyen, E. Pirogova, K. Khoshmanesh and S. Baratchi, *Front. Bioeng. Biotechnol.*, 2019, **7**, 452961.
11 D. B. Camasão and D. Mantovani, *Mater. Today Bio*, 2021, **10**, 100106.
12 N. V. Menon, H. M. Tay, S. N. Wee, K. H. H. Li and H. W. Hou, *Lab Chip*, 2017, **17**, 2960–2968.
13 Y. Nashimoto, T. Hayashi, I. Kunita, A. Nakamasu, Y. S. Torisawa, M. Nakayama, H. Takigawa-Imamura, H. Kotera, K. Nishiyama, T. Miura and R. Yokokawa, *Integr. Biol.*, 2017, **9**, 506–518.
14 C. G. M. van Dijk, M. M. Brandt, N. Poulis, J. Anten, M. van der Moolen, L. Kramer, E. F. G. A. Homburg, L. Louzao-Martinez, J. Pei, M. M. Krebber, B. W. M. van Balkom, P. de Graaf, D. J. Duncker, M. C. Verhaar, R. Luttge and C. Cheng, *Lab Chip*, 2020, **20**, 1827–1844.
15 S. Itai and H. Onoe, *Adv. Healthcare Mater.*, 2022, **11**, 2101509.
16 G. Gao, J. Y. Park, B. S. Kim, J. Jang and D. W. Cho, *Adv. Healthcare Mater.*, 2018, **7**, 1801102.
17 J. Schöneberg, F. De Lorenzi, B. Theek, A. Blaeser, D. Rommel, A. J. C. Kuehne, F. Kießling and H. Fischer, *Sci. Rep.*, 2018, **8**(1), 1–13.
18 Z. Wang, S. M. Mithieux and A. S. Weiss, *Adv. Healthcare Mater.*, 2019, **8**, 1900742.
19 L. Wan, J. Flegle, B. Ozdoganlar and P. R. Leduc, *Micromachines*, 2020, **11**, 907.
20 S. Li, H. Li, X. Shang, J. He and Y. Hu, *MedComm: Biomater. Appl.*, 2023, **2**, e46.
21 M. K. Gelber and R. Bhargava, *Lab Chip*, 2015, **15**, 1736–1741.
22 W. Huang Goh, M. Hashimoto, W. H. Goh and M. Hashimoto, *Macromol. Mater. Eng.*, 2018, **303**, 1700484.
23 P. Yin, B. Hu, L. Yi, C. Xiao, X. Cao, L. Zhao and H. Shi, *Micromachines*, 2018, **9**, 327.
24 J. B. Nielsen, R. L. Hanson, H. M. Almughamsi, C. Pang, T. R. Fish and A. T. Woolley, *Anal. Chem.*, 2020, **92**, 150–168.

25 N. Contessi Negrini, M. Bonnetier, G. Giatsidis, D. P. Orgill, S. Farè and B. Marelli, *Acta Biomater.*, 2019, **87**, 61–75.
26 S. Li, K. Wang, X. Jiang, Q. Hu, C. Zhang and B. Wang, *ACS Biomater. Sci. Eng.*, 2020, **6**, 2297–2311.
27 J. S. Miller, K. R. Stevens, M. T. Yang, B. M. Baker, D. H. T. Nguyen, D. M. Cohen, E. Toro, A. A. Chen, P. A. Galie, X. Yu, R. Chaturvedi, S. N. Bhatia and C. S. Chen, *Nat. Mater.*, 2012, **11**(9), 768–774.
28 H. M. Eltaher, F. E. Abukunna, L. Ruiz-Cantu, Z. Stone, J. Yang and J. E. Dixon, *Acta Biomater.*, 2020, **113**, 339–349.
29 A. Tocchio, M. Tamplenizza, F. Martello, I. Gerges, E. Rossi, S. Argentiere, S. Rodighiero, W. Zhao, P. Milani and C. Lenardi, *Biomaterials*, 2015, **45**, 124–131.
30 A. Shimizu, W. H. Goh, S. Itai, M. Hashimoto, S. Miura and H. Onoe, *Lab Chip*, 2020, **20**, 1917–1927.
31 A. Shimizu, W. H. Goh, S. Itai, R. Karyappa, M. Hashimoto and H. Onoe, *Biomicrofluidics*, 2020, **20**, 1917–1927.
32 B. Pan, L. Shao, J. Jiang, S. Zou, H. Kong, R. Hou, Y. Yao, J. Du and Y. Jin, *Mater. Des.*, 2022, **222**, 111012.
33 S. Sasaki, T. Suzuki, K. Morikawa, M. Matsusaki and K. Sato, *Micromachines*, 2023, **14**, 107.
34 Y. Liu, Y. Zhang, W. Jiang, Y. Peng, J. Luo, S. Xie, S. Zhong, H. Pu, N. Liu and T. Yue, *Micromachines*, 2019, **10**, 275.
35 D. Wang, S. Maharjan, X. Kuang, Z. Wang, L. S. Mille, M. Tao, P. Yu, X. Cao, L. Lian, L. Lv, J. J. He, G. Tang, H. Yuk, C. K. Ozaki, X. Zhao and Y. S. Zhang, *Sci. Adv.*, 2022, **8**, 6900.
36 B. Önal, D. Özen, B. Demir, D. Gezen Ak, E. Dursun, C. Demir, A. G. Akkan and S. Özyazgan, *Curr. Pharm. Biotechnol.*, 2019, **21**, 710–719.
37 D. Shishkova, V. Markova, M. Sinitsky, A. Tsepokina, A. Frolov, N. Zagorodnikov, L. Bogdanov and A. Kutikhin, *Int. J. Mol. Sci.*, 2020, **21**, 8032.
38 K. Kasahara, J. Muramatsu, Y. Kurashina, S. Miura, S. Miyata and H. Onoe, *Sci. Adv.*, 2023, **9**, eadf9917.
39 Y. Kurashina, S. Kurihara, T. Kubota, S. Takatsuka, M. Hirabayashi, H. Shimmura, H. Miyahara, A. Hioki, Y. Matsushita, J. Muramatsu, Y. Ogawa, M. Fujioka, H. J. Okano and H. Onoe, *Adv. Healthcare Mater.*, 2024, 2303546.
40 A. M. W. Bartosch, R. Mathews, M. M. Mahmoud, L. M. Cancel, Z. S. Haq and J. M. Tarbell, *Sci. Rep.*, 2021, **11**(1), 1–12.
41 E. Chuntharpursat-Bon, O. V. Povstyan, M. J. Ludlow, D. J. Carrier, M. Debant, J. Shi, H. J. Gaunt, C. C. Bauer, A. Curd, T. Simon Futers, P. D. Baxter, M. Peckham, S. P. Muench, A. Adamson, N. Humphreys, S. Tumova, R. S. Bon, R. Cubbon, L. Lichtenstein and D. J. Beech, *Commun. Biol.*, 2023, **6**(1), 1–18.
42 L. Ramage, *Cell Health Cytoskeleton*, 2012, **4**, 1–9.
43 A. N. Gasparski and K. A. Beningo, *Arch. Biochem. Biophys.*, 2015, **586**, 20–26.
44 K. Sughimoto, Y. Shimamura, C. Tezuka, K. Tsubota, H. Liu, K. Okumura, Y. Masuda and H. Haneishi, *Heart Vessels*, 2016, **31**, 1168–1175.
45 H. Cheng, W. Zhong, L. Wang, Q. Zhang, X. Ma, Y. Wang, S. Wang, C. He, Q. Wei and C. Fu, *Biomed. Pharmacother.*, 2023, **158**, 114198.
46 E. P. Béguin, E. F. J. Janssen, M. Hoogenboezem, A. B. Meijer, A. J. Hoogendijk and M. van den Biggelaar, *Mol. Cell. Proteomics*, 2020, **19**, 1179–1192.
47 S. Okazaki, *Microelectron. Eng.*, 2015, **133**, 23–35.
48 V. R. Manfrinato, A. Stein, L. Zhang, C. Y. Nam, K. G. Yager, E. A. Stach and C. T. Black, *Nano Lett.*, 2017, **17**, 4562–4567.
49 Q. K. Li, Y. Xiao, H. Liu, H. L. Zhang, J. Xu and J. H. Li, *Opt. Commun.*, 2019, **434**, 1–6.
50 S. Wang, Z. Yang, Z. Li and Y. Tian, *J. Microbiol. Biotechnol.*, 2020, **30**, 1082.
51 T. Tezel and V. Kovan, *Rapid Prototyp. J.*, 2022, **28**, 185–194.
52 P. Czyżewski, D. Marciniak, B. Nowinka, M. Borowiak and M. Bieliński, *Polymers*, 2022, **14**, 356.
53 V. A. Beck, N. N. Watkins, A. S. Ashby, A. A. Martin, P. H. Paul, J. R. Jeffries and A. J. Pascall, *Phys. Fluids*, 2020, **32**, DOI: **10.1063/5.0029438/13382148/112020_1_ACCEPTED_MANUSCRIPT.PDF**.
54 M. A. Skylar-Scott, S. G. M. Uzel, L. L. Nam, J. H. Ahrens, R. L. Truby, S. Damaraju and J. A. Lewis, *Sci. Adv.*, 2019, **5**, DOI: **10.1126/SCIADV.AAW2459/SUPPL_FILE/AAW2459_SM.PDF**.
55 W. F. Hynes, M. Pepona, C. Robertson, J. Alvarado, K. Dubbin, M. Triplett, J. J. Adorno, A. Randles and M. L. Moya, *Sci. Adv.*, 2020, **6**, DOI: **10.1126/SCIADV.ABB3308/SUPPL_FILE/ABB3308_SM.PDF**.
56 D. R. Myers and W. A. Lam, *Annu. Rev. Biomed. Eng.*, 2021, **23**, 407–432.
57 S. Fleischer, D. Naveed Tavakol, G. Vunjak-Novakovic, S. Fleischer, D. N. Tavakol and G. Vunjak-Novakovic, *Adv. Funct. Mater.*, 2020, **30**, 1910811.
58 B. D. M. Chaparro-Rico, F. Sebastiano and D. Cafolla, *Machines*, 2020, **8**, 81.
59 D. Lopes, R. Agujetas, H. Puga, J. Teixeira, R. Lima, J. P. Alejo and C. Ferrera, *Int. J. Mech. Sci.*, 2021, **207**, 106650.